Fachtagung "Experimentelle Strömungsmechanik"
7.–9. September 2021, Bremen

Numerische und experimentelle Untersuchung des Strömung in einem Blasensäulenreaktor

Numerical and experimental investigation of fluid flow in a bubble column reactor

Giovanni Luzi[1], Christopher McHardy[2], Bastian Eysel[2], Christoph Lindenberger[3], Cornelia Rauh[1,2], Antonio Delgado[1,4]

[1]LSTME Busan Branch, Busan 46742, Republic of Korea
[2]Department of Food Biotechnology and Food Process Engineering, Technische Universität Berlin, 14195 Berlin, Germany
[3]OTH Amberg-Weiden, Department of Mechanical Engineering and Environmental Engineering, 92241 Amberg, Germany
[4]Institute of Fluid Mechanics, University of Erlangen-Nuremberg, 91058 Erlangen, Germany

Blasensäule, Bioreaktor, Numerische Simulation, Homogeneous Regime, Computational Fluid Dynamics
Bubble column reactors, Bioreactors, Numerical Simulations, Homogeneous Regime, Computational Fluid Dynamics

Abstract

Bubble columns find wide application as multiphase contactors and reactors in chemical, biochemical, metallurgical, and petrochemical industries due to their ease of operation and maintenance, high heat and mass transfer rates, and low operating and maintenance costs. In those reactors, gas is usually introduced from a sparger at the bottom of a column filled with liquid. Over the years, the computational capacity has increased considerably, and computational fluid dynamics (CFD) models that can simulate the multiphase flow have been consistently improved. In principle, numerical simulations are highly requested and desirable since they can provide a valid predictive tool compared to costly experiments. Nevertheless, the outcomes of numerical simulations need to be validated with experimental results to prove their validity. In this regard, we simulate the two-phase flow in the homogeneous regime of a bubble column reactor with a cylindrical cross-section utilizing the open-source software OpenFOAM®. Afterward, we compare the numerical profiles of the time-averaged axial liquid velocity with the experimental ones obtained with a low-cost Particle Image Velocimetry (PIV) system at different heights of the column. In general, we find a reasonable agreement between numerical and experimental data for different values of the turbulent Schmidt number.

Introduction

The processes involving two-phase flows, or more in general multiphase flows frequently occur in reactor operations. Among the variety of reactor types, bubble columns are among the most used ones in industry. They possess unique properties including simplicity of design and maintenance, excellent heat and mass transfer characteristics at low energy input, easy temperature control, and absence of moving mechanical parts which entails very competitive investment and maintenance costs (Deckwer and Schumpe. 1993). Thereby, they find wide applications in chemical, petrochemical, biological, and biotechnological industries, only to cite a few.

GALA e.V., Karlsruhe, Germany, ISBN 978-3-9816764-7-1

Nowadays, numerical simulations of bubble column flows are considered a powerful tool to study the complex physical phenomena occurring while bubble column reactors are in operation. In this regard, Computational Fluid Dynamics (CFD) plays a decisive role since it is considered a valid predictive tool compared to an expensive experimental setup. However, the modeling of two-phase flow is not a trivial task and intense investigations are undergoing for the last twenty years.

Two-dimensional simulations of bubble column flows may deliver results in a relatively short time, since they are computationally less expensive compared to three-dimensional ones. Therefore, they are very useful to test new models or implement new approaches. For instance, (Vikas et al. 2011) implemented a Quadrature-Based Moment Methods (QBMM) in a two-way coupled flow solver. Specifically, the authors solved the incompressible Navier-Stokes equations for the liquid phase and moment transport equations for the dispersed bubble phase considering a two-dimensional bubble column. They performed numerical simulations for different gas flow rates, always observing a meandering behavior of the bubble plume. (Buffo et al. 2013) implemented the Cumulative Quadrature Method of Moments (CQMOM) and the Direct Quadrature Method of Moments (DQMOM) in the commercial software Ansys Fluent 13 to simulate the fluid flow of a two-dimensional bubble column considering bubble coalescence, break-up, and mass transfer. Moreover, they compared the results obtained with the CQMOM and the DQMOM with those obtained with the Direct Simulation Monte Carlo (DSMC) method. The computational time required by both the CQMOM and the DQMOM is significantly lower compared to the one required by the DSMC. Besides, the CQMOM is found to be a very stable and efficient algorithm.

However, the results obtained by two-dimensional simulations may be unrealistic (Mudde and Simonin. 1999), and highly grid size dependent (Bech 2005). In contrast to that, only three-dimensional simulations can reproduce the typical complex flow patterns of a bubble column reactor (Pfleger and Becker. 2001; Chen et al. 2004). However, the interphase forces need to be included in the numerical model and the choice of the most adequate correlation is critical to obtain predictions that agree with experimental results. In this regard, (Masood et al. 2014) compared the outcomes obtained with different turbulent closure and drag force models. Besides, they performed a comprehensive investigation concerning how different interphase force models affect the flow field. In a different contribution, (Asad et al. 2017) utilized the discrete bubble model (DBM) coupled with the volume of fluid (VOF) method to investigate the hydrodynamics of a rectangular bubble column. They tested three different drag models and three different injection conditions. They found that the time-averaged vertical component of the liquid velocity and the time-averaged vertical component of the gas velocity agree reasonably well with the experimental results of (Deen et al. 2000) for all the different drag models and injection conditions. However, the instantaneous flow field of the disperse phase differs considerably depending on the inlet. In cases of higher values of gas superficial velocities, coalescence and break-up phenomena have been considered as well. (Chen et al. 2004) simulated the heterogeneous two-phase flow by discretizing the gas phase into n-classes depending on the bubble size. They solved a transport equation for each class together with a two-fluid model called the Algebraic Slip Mixture Model (ASMM) to compute the local number density for each bubble class. Numerical results of three-dimensional simulations agree well with experimental ones performed with the Computed Automated Radiative Particle Tracking (CARPT) technique in terms of the profile of the time-averaged axial component of the liquid velocity and the one of the gas-hold-up.

In a different contribution, (Vieira et al. 2018) also simulated the fluid flow of a rectangular bubble column reactor, modeling coalescence and break-up phenomena employing the Quadrature-Method of Moments (QMOM). They compared the outcomes of three different RANS $k-\varepsilon$ models, namely the standard, the modified and the mixture one, concluding that the choice of the turbulence model strongly affects the predictions of the dissipation rates, while the selection of the lift model is crucial for the correct determination of the gas hold-up and the time-averaged vertical component of the liquid velocity profile.

GALA e.V., Karlsruhe, Germany, ISBN 978-3-9816764-7-1

In the present contribution, we simulate the two-phase fluid flow of a reactor equipped with a dip-tube sparger utilizing the open-source software OpenFOAM®, and we compare the time-averaged vertical component of the liquid velocity profile at different heights obtained numerically with the one obtained experimentally with a low-cost PIV equipment. We find a reasonable agreement between the results obtained numerically and experimentally by properly tuning the value of the turbulent Schmidt number.

Simulation set-up

Geometry and grid

We consider a reactor with a cylindrical cross-section and a dip-tube sparger located at the bottom of it. The lower part of the reactor has a rounded shape, see Fig. 1a). The whole height of the reactor is 46 [cm] and the diameter of the cylindrical cross-section is 7 [cm]. The height of the liquid level is 39 [cm] above the reactor base.

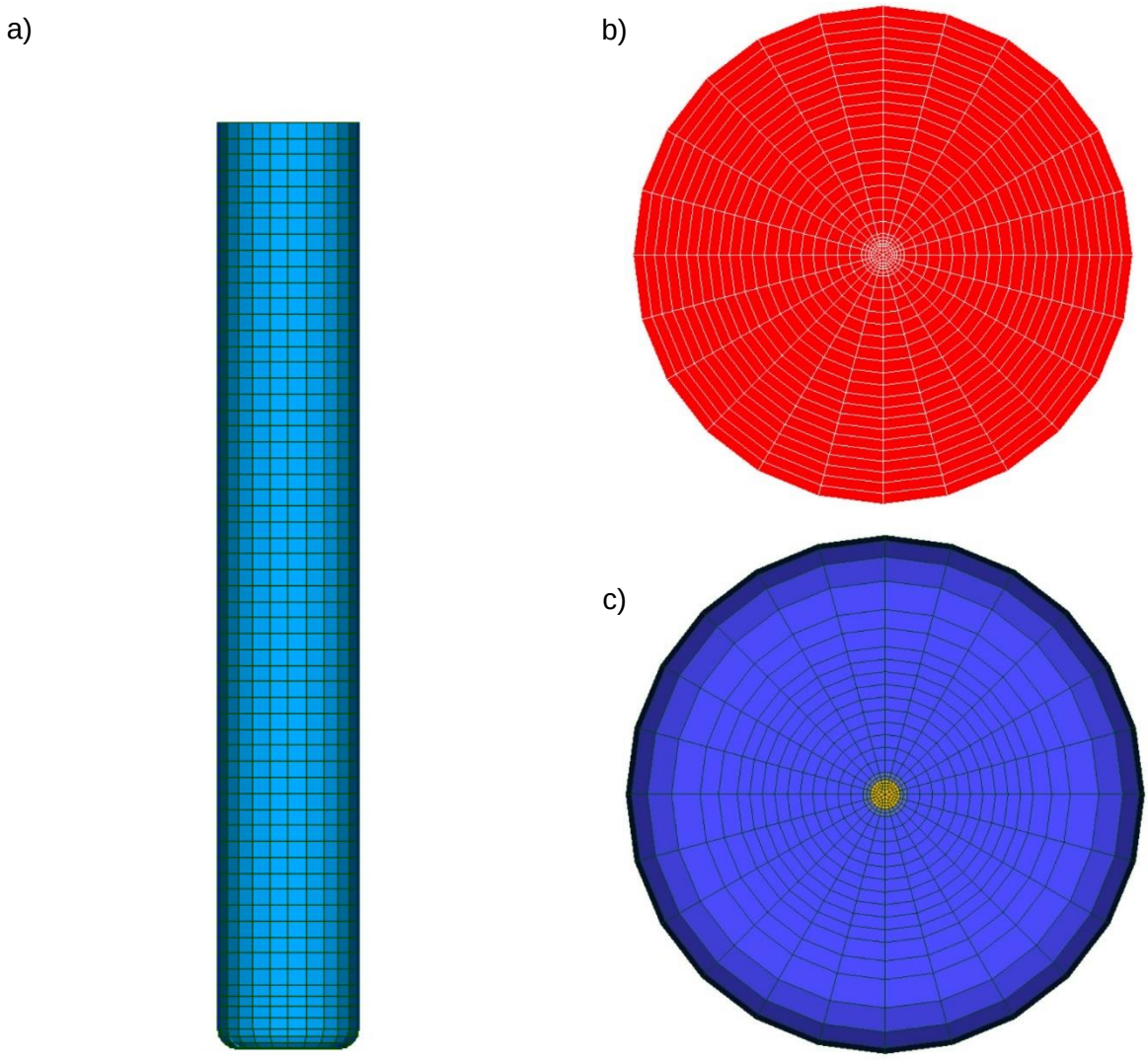

Fig. 1 a) vertical view: structured mesh with 35664 elements, b) detailed view of the meshed outlet, and c) detailed view of the mesh in the lower part of the reactor. The yellow portion of the mesh represents the inlet, located at 3.2 [cm] from the bottom of the reactor.

GALA e.V., Karlsruhe, Germany, ISBN 978-3-9816764-7-1

The dip-tube sparger has also a cylindrical cross-section whose diameter is 4 [mm] and its height is 3.2 [cm]. Both the geometry and the grid have been created using the open-source software SALOME. The domain is covered with a coarse hexahedral structured grid containing 35664 volumes. The details of the mesh are shown in Fig. 1a), b), and c).

Mathematical modeling of fluid flow

We employ the Eulerian-Eulerian formulation to model the two-phase flow of the bubble column reactor where each phase has its mass and conservation equation. The mass conservation equation for both phases k reads

$$\frac{\partial}{\partial t}\left(\rho_k \alpha_k\right) + \nabla \cdot \left(\rho_k \alpha_k \boldsymbol{u}_k\right) = 0 \tag{1}$$

where, α_k , ρ_k and $\boldsymbol{u}_k$ represent the volume fraction, density, and velocity of each phase, respectively. In Eq. (1) $k = G, L$, where *L* stands for liquid and *G* for gas. The momentum equations for both phases are

$$\frac{\partial}{\partial t}\left(\rho_k \alpha_k \boldsymbol{u}_k\right) + \nabla \cdot \left(\rho_k \alpha_k \boldsymbol{u}_k \boldsymbol{u}_k\right) = \nabla \cdot \left(\alpha_k \boldsymbol{\tau}_k\right) - \alpha_k \nabla p + \rho_k \alpha_k \boldsymbol{g} + \boldsymbol{M}_{s,k} \tag{2}$$

where $k = L, G$ again and $s = L, G$ too. The terms on the left-hand side of Eq. 2 indicate the temporal and the convective inertial acceleration of each phase. The terms on the right-hand side are the divergence of the viscous stress tensor of each phase, the pressure gradient shared by both phases, the gravitational and interphase forces, respectively. The stress tensor reads

$$\boldsymbol{\tau}_k = \mu_{k,eff}\left[\nabla \boldsymbol{u}_k + \left(\nabla \boldsymbol{u}_k\right)^T - \frac{2}{3}\mathbf{I}\left(\nabla \cdot \boldsymbol{u}_k\right)\right] \tag{3}$$

Herein, the effective dynamic viscosity $\mu_{k,eff}$ is the sum of the molecular and the turbulent viscosity, i.e.

$$\mu_{k,eff} = \mu_{k,Lam} + \mu_{k,Turb} \tag{4}$$

The term corresponding to the interphase forces $\boldsymbol{M}_{s,k}$ incorporates the drag, lift, virtual mass, wall lubrication, and turbulent dispersion forces. We employ the Ishii Zuber correlation to compute the drag coefficient C_D. The Ishii-Zuber model differentiates three regimes, i.e. the viscous, the distorted particle, and the churn-turbulent one, for more details see (Ishii and Zuber. 1979). Concerning the lift force, we utilize the Tomiyama model (Tomiyama et al. 2002) to compute the lift force coefficient C_L. It reads

$$C_L = \begin{cases} \min\left[0.288\tanh\left(0.121\mathrm{Re}_P, f\left(Eo'\right)\right)\right] & Eo' < 4 \\ f\left(Eo'\right) & 4 < Eo' < 10 \\ -0.27 & Eo' > 10 \end{cases} \tag{5}$$

where, $f\left(Eo'\right) = 0.00105Eo'^3 - 0.0159Eo'^2 - 0.0204Eo' + 0.474$ and Eo' is the Eötvös number computed using the longest axis of a deformable bubble.

The virtual mass force represents the force required to accelerate the mass of the continuous phase near a bubble. We use a fixed value of the virtual mass coefficient, i.e. $C_{VM} = 0.5$.

GALA e.V., Karlsruhe, Germany, ISBN 978-3-9816764-7-1

Concerning the wall lubrication force, we employ the Frank model to compute the wall lubrication force coefficient C_{WL} (Frank et al. 2008), which is

$$C_{WL} = C_W \max\left(0, \frac{1}{C_{WD}} \frac{1 - y_w/(C_{wc} d_B)}{y_w \left(y_w/(C_{wc} d_B)\right)^{p-1}}\right) \tag{6}$$

where $C_{WD} = 6.8$, $C_{WC} = 10.0$ and $p = 1.7$. C_W is a coefficient that is also a function of the Eötvös number.

Finally, we utilize the Favre averaged model (Burns et al. 2004) to calculate the turbulent dispersion forces:

$$\boldsymbol{F}_{L,G}^{TD} = -\bar{C}_{GL} \frac{\nu_{L,Turb}}{\sigma_{L,Turb}} \left(\frac{1}{\bar{\alpha}_G} + \frac{1}{\bar{\alpha}_L}\right) \nabla \bar{\alpha}_L \tag{7}$$

To compute the turbulent eddy viscosity $\mu_{k,Turb}$ of each phase, we selected the mixture $k-\varepsilon$ model (Bezhadi et al. 2004) for both phases.

Simulation details

In this section, we will briefly summarize the main settings and boundary conditions utilized in the simulations. We specify the value of the mass flow rate of the dispersed phase at the inlet, while at the outlet we impose the boundary condition *pressureInletOutletvelocity* for the velocity field, and *InletOutlet* for the k, ε, k_m and ε_m fields. Besides, we set a no-slip boundary condition for the velocity of both fluids, zero gradient boundary condition for k_m and ε_m, and the wall functions implemented in OpenFOAM® for both k and ε at the walls. On top of the reactor, we leave an air headspace of 7 [cm]. Furthermore, we set a constant fixed mean bubble diameter, $d_B = 7.8$ [mm] obtained by solving numerically the governing equation of bubble formation out of a nozzle of (Gaddis and Vogelpohl. 1985). The discretization of gradient, divergence, and Laplacian terms of the governing equations are based on Gauss types of schemes. On the one hand, the Poisson equation of the pressure is solved by using the Geometric-Algebraic Multi-Grid solver implemented in OpenFOAM®. On the other hand, the coupling between the pressure and the velocity field is accomplished using the PIMPLE algorithm. Finally, we integrate all the governing equations in time utilizing an implicit Euler scheme, using an adaptive time step based on the maximum value of the Courant number. We run all the simulations up to $t = 900$ [s] since this time interval is necessary and sufficient for the time averaging.

PIV measurements

We validated the numerical outcomes with experimental data obtained using 2D2C Particle Image Velocimetry. The reactor used in the experiments is shown in Fig. 2a). Gas supply was controlled with a thermal mass flow controller (GF40, Brooks Instrument, Dresden, Germany). We recorded images for the PIV measurements in single-frame mode with a FASTCAM Mini AX100 (Photron, Tokyo, Japan) high-speed camera, equipped with a 50 [mm] 1:1.4 television lens (Cosmicar, Tokyo, Japan). To avoid distortion effects, we located the reactor in a 30 cm x 30 [cm] water tank and aligned it using a spirit level. We set the image size to 512 x 512 pixels, to improve the utilization of the storage capacity of the camera. The light was generated by a 100 [mW] line laser module (MediaLas Electronics GmbH, Balingen Germany) having a wavelength of 650 [nm], and a plane convex lens was used to focus the light beam. Besides, this lens was provided with a diaphragm to generate a defined light section with a thickness of

GALA e.V., Karlsruhe, Germany, ISBN 978-3-9816764-7-1

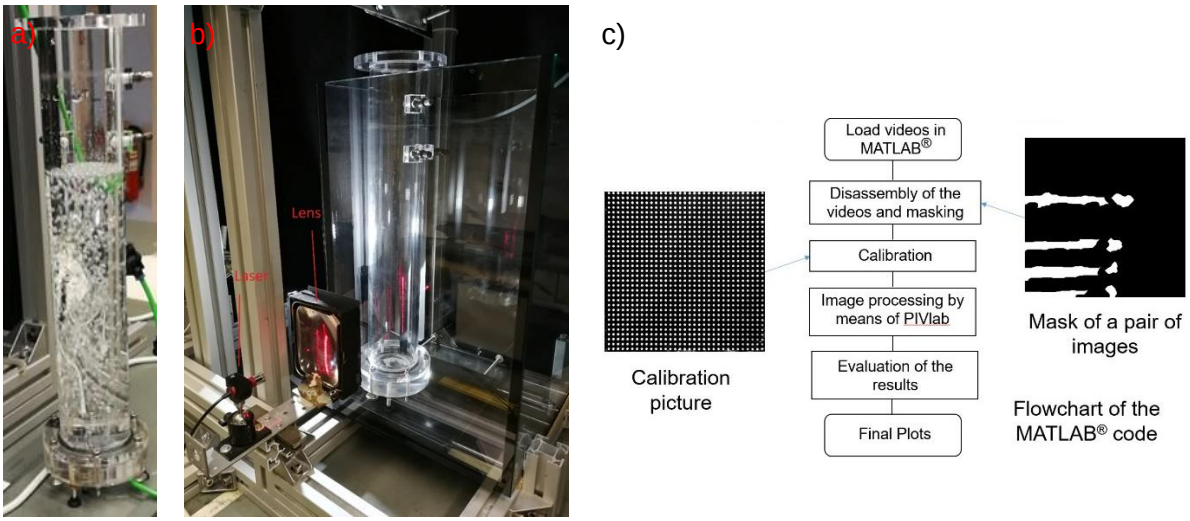

Fig. 2 a) bubble column in operation, b) detailed view of the set-up used for the experiments, including the laser, the lens, and the reactor within the aquarium, c) Schematic flowchart of the image processing steps carried out with MATLAB®.

1 [mm]. The whole setup including the laser, the lens, and the reactor in the aquarium is shown in Fig. 2b).

We utilized VESTOSINT 2157 PMMA particles as tracer particles (Evonik, Darmstadt, Germany) having an average size of 50 [µm] and density of 1016 [kg /m^3]. Calibration images were recorded before the measurements. For this, we manufactured a disk provided with points of 1.5 [mm] diameter, arranged at 2 [mm] from each other. Calibration images were obtained by placing the disk into the water-filled column. For the flow analysis, 875 batches of 50 images were recorded over a total time of 29:10 minutes. The recording of single batches was initiated with a trigger signal after a time interval of 2 seconds to ensure that the recorded flow structures were uncorrelated.

The PIV recordings were processed with MATLAB® using the PIVlab toolbox. An algorithm was developed for the automatic masking of bubbles and reflections and integrated into PIVlab. The algorithm is based on the evaluation of local intensities and object sizes. Accordingly, detected objects on binarized images being larger than 150 pixels were masked out. After detecting erroneous objects, holes in the created masks were filled and dilatation was applied to smooth the object contours. Subsequently, image preprocessing was applied to improve the particle images. The image preprocessing consists of Contrast Limited Adaptive Histogram Equalization (CLAHE) with a kernel size of 50 px and intensity capping with the maximum value set to 0.9. The processed images were used to compute the vector fields in the unmasked regions. Outlier vectors were defined as vectors whose magnitudes deviate from the local average value by more than 3 standard deviations and excluded from the computation of the time-averaged flow velocities. The physical vector magnitudes were estimated by applying the calibration to the computed results.

Results and discussion

In a bubble column reactor, air bubbles form a typical meandering “plume” that promotes displacements of the liquid phase. We also obtain strong oscillations of the disperse phase in our simulations. However, since similar results are reported in our previous publications (McHardy et al. 2018, Luzi et al. 2019) and they will not be presented here. Instead, we directly confront and discuss the outcomes of the numerical results and the experimental data. Specifically, in Fig. 3 we compare the time-averaged vertical component of the liquid velocity at two different heights inside the reactor. The heights are measured from the bottom of the reactor, and they

GALA e.V., Karlsruhe, Germany, ISBN 978-3-9816764-7-1

are $y = 6.6$ [cm] 3a) and $y = 22.2$ [cm] 3b). Numerical simulations correctly reproduce the liquid flow-up in the center of the reactor and the downward flow close to the walls both in the lower part of the reactor close to the sparger and in the middle of it, following the same trend of the experimental results. In the numerical simulations, bubbles tend to concentrate in the center of the reactor since the lift force correlation of Tomiyama foresees a change of the sign when the bubble diameter exceeds the value of approximately 5.8 [cm]. More specifically, bubbles are more concentrated in the center of the reactor close to the sparger where they form, while moving upward they tend to spread forming a more distributed profile. This trend is also confirmed by the experimental results, see Fig. 3a) and 3b). Numerical results obtained with $\sigma_{L,Turb} = 1$ highly overestimate the experimental data close to the sparger, being the peak of the numerical result located at approximately $u_{yL,Tav} = 0.24$ [m/s], while the maximum values of the experimental results are approximately $u_{yL,Tav} = 0.16$ [m/s], see Fig. 3a). However, in the middle of the reactor numerical and experimental data are closer, see Fig. 3b). By decreasing the value of $\sigma_{L,Turb}$, numerical outcomes gradually approach the experimental data in the lower part of the reactor, see Fig. 3a). This can be explained by the fact that by decreasing the value of $\sigma_{L,Turb}$ the turbulent dispersion forces of the liquid phase are enhanced. Those cause bubbles to spread from the central part of the reactor toward regions of lower concentration, thereby reducing the momentum exchange between the disperse and the liquid phase. Therefore, the peak of the velocity profile of the liquid phase gradually reduces close to the sparger as the turbulent Schmidt number is increased, see Fig. 3a). On the one hand, experimental results are not perfectly symmetric, see Fig. 3a) and 3b). As indicated by the literature, even slight inclinations of 0.5° can affect the flow profile significantly (Sommerfeld 2004) which might explain the experimental observations as a perfect alignment of the reactor could not be ensured. On the other hand, numerical results are not symmetric since the mesh is coarse and it needs to be refined close to the reactor center, especially in the case of lower values $\sigma_{L,Turb}$. Also, at the position $y = 22.2$ [cm], the peak of the time-averaged liquid velocity profile varies by increasing the turbulent Schmidt number. However, the maximum value of the peak decreases not always by decreasing the value of the turbulent Schmidt number. For instance, we find that the peak of the liquid velocity profile obtained numerically utilizing $\sigma_{L,Turb} = 0.6$ is higher than those obtained using $\sigma_{L,Turb} = 1$ and $\sigma_{L,Turb} = 0.8$, see Fig. 3b). Similarly, the peak of the velocity profile of the liquid phase obtained numerically using $\sigma_{L,Turb} = 0.4$ is higher than the one obtained using $\sigma_{L,Turb} = 0.5$, see Fig. 3b). This can be explained by the complex nonlinear interaction between the interphase forces, especially the lift and the turbulent dispersion ones. On the one hand, lift forces push bubbles toward the center of the reactor. On the other hand, due to the turbulent dispersion forces, bubbles migrate from regions of higher concentrations toward regions of lower concentrations. Therefore, the effects of this nonlinear interaction determine the resulting time-averaged velocity profile of the liquid phase.

Conclusion

In this work, we compared the time-averaged profile of the vertical liquid velocity obtained with OpenFOAM® and the one obtained experimentally for the case of a cylindrical reactor operating in the monodisperse regime at a low value of gas superficial velocity, i.e., $u_g = 1.86$ [mm/s]. In general, the outcomes of the simulations show good accordance with the experimental results and the agreement between them can be improved by properly tuning the turbulent

GALA e.V., Karlsruhe, Germany, ISBN 978-3-9816764-7-1

Schmidt number. Besides, the main features of the bubble column flow are successfully reproduced, like for instance, the typical meandering bubble plume of a bubble column reactor. However, the complex interactions that determine the velocity profile are not completely understood, especially in the upper part of the reactor. Therefore, further research is needed to clarify the interplay among the interphase forces, especially between the lift and the turbulent dispersion ones. Besides, the present experimental data have been obtained with low-cost PIV equipment and further experiments will be performed in the future with a professional PIV set-up to validate the present ones.

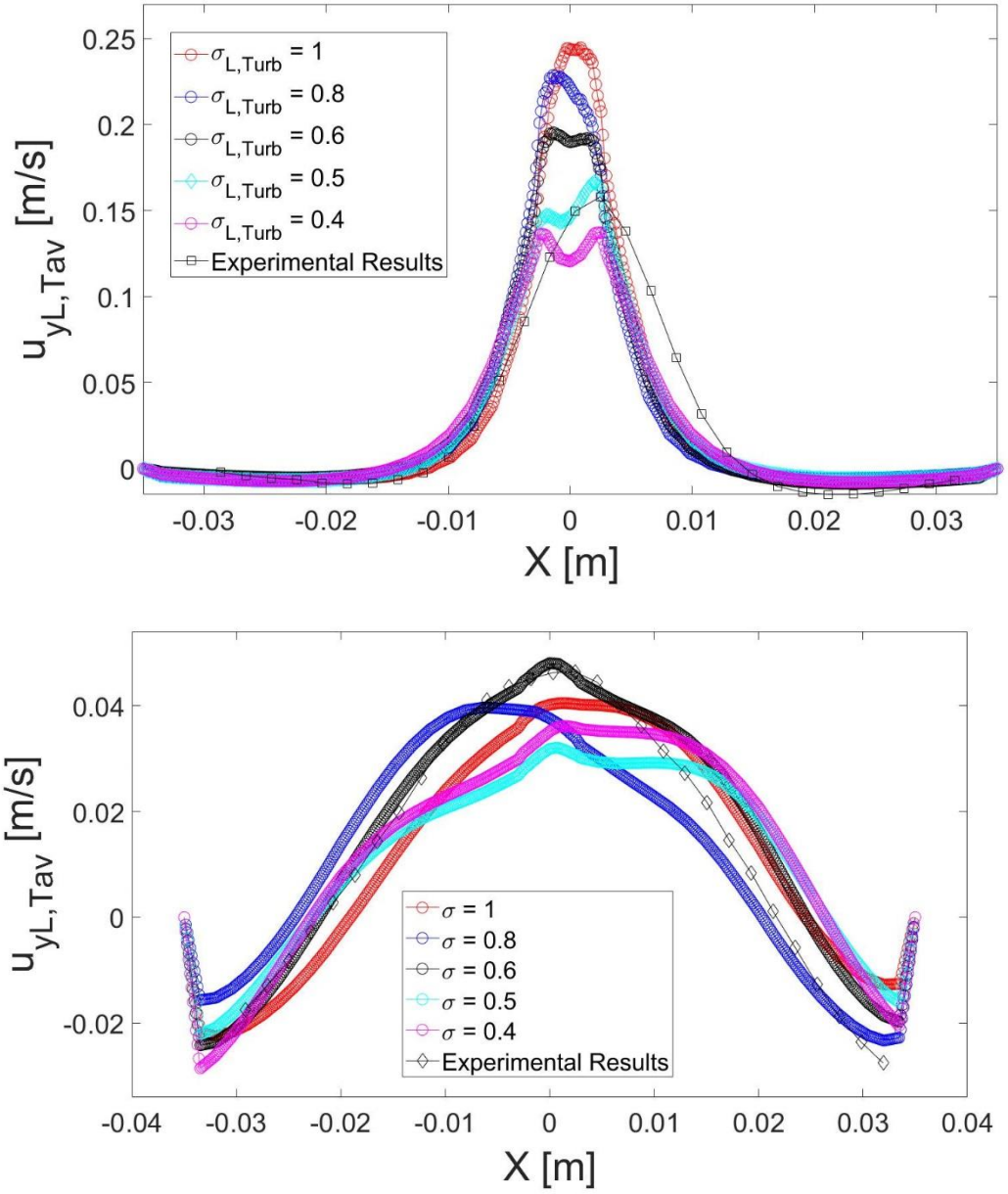

Fig. 3) Time-averaged vertical component of the liquid velocity on a x-y plane at z=0. y = 6.6 [cm] a) and y = 22.2 [cm] b). The gas superficial velocity is 1.86 [mm/s].

Literature

Deckwer, W.-D., Schumpe A., 1993: "Improved tools for bubble column reactor design and scale-up", Chemical Engineering Science, 48, pp. 889–911

Vikas, V., Yuan, C., Wang, Z.J., Fox, R.O., 2011: "Modeling of bubble-column flows with quadrature-based moment methods", Chemical Engineering Science, 66, pp. 3058–3070

GALA e.V., Karlsruhe, Germany, ISBN 978-3-9816764-7-1

Buffo, A., Vanni, M., Marchisio, D.L., Fox R.O., 2013: "Multivariate Quadrature-Based Moments Methods for turbulent polydisperse gas–liquid systems", International Journal of Multiphase Flow, 50, pp. 41–57
Mudde, R.F., Simonin O., 1999: "Two- and three-dimensional simulations of a bubble plume using a two-fluid model", Chemical Engineering Science, 54, pp. 5061–5069
Bech, K., 2005: "Dynamic simulation of a 2D bubble column", Chemical Engineering Science, 60, pp. 5294–5304
Pfleger, D., Becker, S., 2001: "Modelling and simulation of the dynamic flow behaviour in a bubble column", Chemical Engineering Science, 56, pp. 1737–1747
Chen, P., Sanyal, J., Dudukovic, M.P., 2004: "CFD modeling of bubble columns flows: implementation of population balance", Chemical Engineering Science, 59, pp. 5201–5207
Masood, R.M.A, Rauh, C., Delgado, A., 2014: "CFD simulation of bubble column flows: An explicit algebraic Reynolds stress model approach", International Journal of Multiphase Flow, 66, pp.11–25
Asad, A., Kratzsch, C., Schwarze, R., 2017: "Influence of drag closures and inlet conditions on bubble dynamics and flow behavior inside a bubble column", Engineering Applications of Computational Fluid Mechanics, 11, pp. 127–141
Deen N., Hjertager H. B., Tron, S., 2000: "Comparison of PIV and LDA Measurement Methods Applied to the Gas-Liquid Flow in a Bubble Column", 10th International Symposium on Application of Laser Techniques to Fluid Mechanics, Lisbon, Portugal, pp. 1–11
Braga Vieira, C., Litrico, G., Askari, E., Lemieux, G., Proulx, P., 2018: "Hydrodynamics of Bubble Columns: Turbulence and Population Balance Model", ChemEngineering, 1, pp. 2-12
Ishii, M., Zuber, N., 1979: "Drag coefficient and relative velocity in bubbly, droplet or particulate flows", AIChE Journal, 25, pp. 843–55
Tomiyama, A., Tamai, H., Zun, I., Hosokawa S., 2002: "Transverse migration of single bubbles in simple shear flows", Chemical Engineering Science, 57, pp. 1849–1858
Frank,T., Zwart, P.J., Krepper, E., Prasser, H.-M., 2008: "Lucas D. Validation of CFD models for mono- and polydisperse air–water two-phase flows in pipes", Nuclear Engineering and Design, 238, pp. 647–659
Burns, A. D., Frank, T., Hamill I., Shi J.-M. 2004: "The Favre Averaged Drag Model for Turbulent Dispersion in Eulerian Multi-Phase Flows", 5th International Conference on Multiphase Flow, ICMF'04 Yokohama, Japan, pp. 1–17
Behzadi, A., Issa, R.I., Rusche, H. 2004: "Modelling of dispersed bubble and droplet flow at high phase fractions", Chemical Engineering Science, 59, pp. 759–770
Gaddis, E.S., Vogelpohl A., 1986: "Bubble formation in quiescent liquids under constant flow conditions", Chemical Engineering Science, 41, pp. 97–105
McHardy, C., Luzi, G., Lindenberger, C., Agudo J.R., Delgado, A., Rauh, C. 2018: "Numerical analysis of the effects of air on light distribution in a bubble column photobioreactor", Algal Research, 31, pp. 311–325.
Luzi, G., McHardy, C., Lindenberger, C., Rauh, C., Delgado, A., 2019: "Comparison between different strategies for the realization of flashing-light effects – Pneumatic mixing and flashing illumination", Algal Research, 38, 101404
Sommerfeld, M., 2004: "Bubbly Flows: Analysis, Modelling and Calculation", Springer-Verlag, Berlin, Heidelberg

GALA e.V., Karlsruhe, Germany, ISBN 978-3-9816764-7-1